Geophys. J. Int. (2009) **179,** 144–153 doi: 10.1111/j.1365-246X.2009.04300.x

Constraints on the mantle temperature gradient along the Southeast Indian Ridge from crustal structure and isostasy: implications for the transition from an axial high to an axial valley

Janet M. Baran,[1,2] James R. Cochran,[1] R. Chadwick Holmes,[1] Maya Tolstoy[1] and Suzanne M. Carbotte[1]

[1] *Lamont-Doherty Earth Observatory of Columbia University,* 61 *Route* 9W*, Palisades,* NY 10964, *USA. E-mail: jrc@ldeo.columbia.edu*
[2] *U.S. Department of Commerce, National Ocean and Atmospheric Administration,* 14th *and Constitution Avenue NW,* Rm. 6121, *Washington,* DC 20230, *USA*

Accepted 2009 June 16. Received 2009 May 18; in original form 2008 August 21

SUMMARY

Axial and ridge flank depths on the Southeast Indian Ridge (SEIR) systematically increase for 2500 km from 90°E to 120°E approaching the Australian-Antarctic Discordance. The SEIR also experiences an abrupt change in ridge axis morphology near 103°30′E with axial highs found to the west and axial valleys to the east. Since the spreading rate is constant throughout this region, these variations have been ascribed to an along-axis gradient in mantle temperature. A seismic refraction experiment provides information on the crustal thickness and seismic velocity structure of two segments with differing axial morphology. Segment P2, centred near 102°E with an axial high has a mean crustal thickness of 5.9 ± 0.2 km, while the mean crustal thickness is 5.3 ± 0.3 km at Segment S1 with an axial valley and centred near 109°45′E. Isostatic compensation of the difference in crustal thickness and density structure between the two segments only accounts for 33 m of the 198 m difference in average ridge flank depth between the two segments. The remaining depth difference must result from a difference in mantle density. Melt production models imply a mantle temperature difference of 11–13.5 °C to produce the observed difference in crustal thickness. Isostatic compensation of the two segments requires that the resulting density difference must extend to about 300 km in the mantle.

The transition in axial morphology along the SEIR is very abrupt occurring over a narrow zone within a single segment in which the transition is complete. If a linear mantle temperature gradient is assumed, the temperature difference across the transition segment is only 2.4 °C. The change in axial morphology is accompanied by abrupt changes in other parameters including abyssal hill height, magnetic anomaly amplitude, layer 2a thickness and the presence or absence of an axial magma lens. The abrupt, coincident change in a number of parameters with a very small change in mantle temperature strongly suggests a threshold change between two distinctly different modes of crustal accretion. The trigger for the transition appears to be whether a steady-state crustal magma lens can be maintained.

Key words: Gravity anomalies and Earth structure; Mid-ocean ridge processes; Crustal structure; Indian Ocean.

INTRODUCTION

The Southeast Indian Ridge (SEIR) is an intermediate-rate spreading centre that separates the Australian and Antarctic plates and extends from the Rodriquez triple junction near 25°S, 70°E to the Macquarie triple junction near 63°S, 165°E. The SEIR undergoes an along-axis transition in axial morphology at about 103°30′E from an axial high to the west to an axial valley to the east (Fig. 1). This transition is not related to a variation in spreading rate, which is nearly constant (69.2–72.2 mm a^{-1}) for 2500 km from 90°E to 120°E (DeMets *et al.* 1994). The section of the ridge axis with an axial valley actually has a slightly higher spreading rate than the section with an axial high.

The portion of the SEIR from 90°E to 120°E is characterized by a long-wavelength west-to-east increase in axial and ridge flank depths (Ma & Cochran 1996; Cochran *et al.* 1997; Sempere *et al.* 1997). This portion of the SEIR is bounded to the east by the Australian-Antarctic Discordance (AAD), a region of deep and chaotic bathymetry extending from 120°E to 127°E (Weissel & Hayes 1974; Sempere *et al.* 1991; Palmer *et al.* 1993). Surface

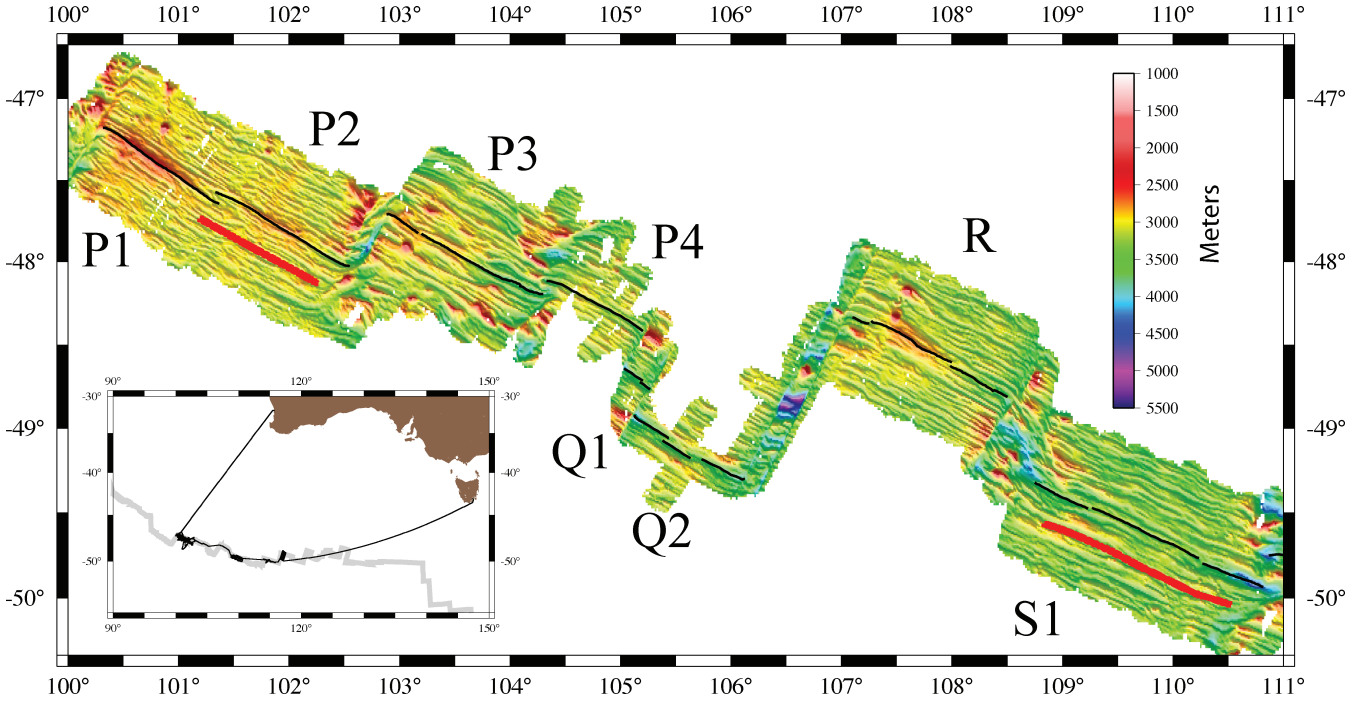

Figure 1. Shaded relief bathymetric map showing the crestal region of the SEIR from 100°E to 111°E. Black lines show the location of the ridge axis with segments labelled. Red lines show the location of the two seismic crustal sections analysed in this study. A transition in axial morphology from an axial high to the west to an axial valley to the east occurs within Segment P3. Bathymetry is gridded multibeam data from *R/V Melville* cruises West09MV and West10MV (Cochran *et al.* 1997; Sempere *et al.* 1997) and is illuminated from the SSW. Inset shows the location of our study area relative to Australia and the ship track for *R/V Maurice Ewing* cruise EW0114.

wave (e.g. Forsyth *et al.* 1987; Kuo 1993) and petrologic (e.g. Klein *et al.* 1991; Pyle 1994) studies suggest that the AAD is underlain by cooler than normal mantle. This is supported by seismic refraction data interpreted as showing a thin crust in the AAD (Tolstoy *et al.* 1995; Kojima *et al.* 2003).

These observations led to the conclusion that the change in axial morphology along the SEIR results from a lateral gradient in mantle temperature. Cochran *et al.* (1997) estimated from bathymetry and gravity data that the mantle temperature could vary by as much as 50–90 °C between 88°E and 114°E, depending on the depth to which the temperature gradient extended. This estimate represents an upper bound on the possible temperature gradient, because it is based on varying only the mantle temperature and does not account for related changes in crustal thickness.

A gradient in mantle temperature along the SEIR is also suggested by basalt chemistry along the ridge. Fig. 2 shows the variation of $Na_{8.0}$ and $Fe_{8.0}$ as a function of longitude for basaltic glasses recovered from the SEIR axis (Mahoney *et al.* 2002). These data show distinct trends of decreasing $Fe_{8.0}$ and increasing $Na_{8.0}$ from west to east along the ridge, implying a decrease in mantle temperature and extent of melting approaching the AAD.

During the Austral Summer of 2001–2002, a multichannel seismic (MCS)/ocean-bottom hydrophone (OBH) experiment was conducted on *R/V Maurice Ewing* along the SEIR between 100°E and 116°E (Fig. 1). In particular, constraints on the crustal velocity structure and thickness were obtained from ridge segments on either side of the transition in axial morphology (Baran *et al.* 2005, 2009; Holmes *et al.* 2008). We will utilize these data to constrain the mantle temperature change between those segments and to investigate the nature of the transition in morphology and crustal structure.

AXIAL MORPHOLOGY OF THE SEIR

A major change in the morphology of the SEIR axis occurs at about 103°30′E within Segment P3 (Fig. 1). Segments west of P3 to about 79°E, near the Amsterdam—St. Paul Plateau, are characterized by an axial high (Cochran *et al.* 1997; Scheirer *et al.* 2000), while segments east of P3 to the eastern boundary of the AAD near 127°E are characterized by an axial valley (Palmer *et al.* 1993; Cochran *et al.* 1997).

The axial highs observed to the west of Segment P3 are primarily 'rifted' axial highs marked by multiple inward-facing faults with throws of <100 m located within 1–2 km of the axis. Well-developed 'EPR-like' axial highs are found at Segments P1 near 101°E and M1 near 89°E. As discussed by Baran *et al.* (2005), these two segments are both located immediately to the east of significant left-stepping transforms and are leading segments in the fixed hot spot reference frame (Gripp & Gordon 1990) which may result in an enhanced melt supply (Carbotte *et al.* 2004). The only segment between 79°E and 103°E with an axial valley is Segment N near 96°E, where the axis is marked by a shallow 200–400 m deep, 6–8-km-wide valley. Segment N is a short 55-km-long segment situated between two large-offset (93 and 40 km) transforms (Cochran *et al.* 1997) and the mantle temperature and melt supply beneath it are probably reduced by lateral heat conduction across the transforms.

Axial valleys to the east of Segment P3 to 114°E are generally 400–800 m deep and 5–15 km wide (Cochran *et al.* 1997; Shah & Sempere 1998). The primary exception is Segment R. The ridge axis in the vicinity of 107°30′E within Segment R is located on a 15–20-km-wide, 300–400-m-high plateau bounded by steep, fault-like scarps. The plateau becomes lower and less distinct to the east and by the eastern end of the segment, the axis is

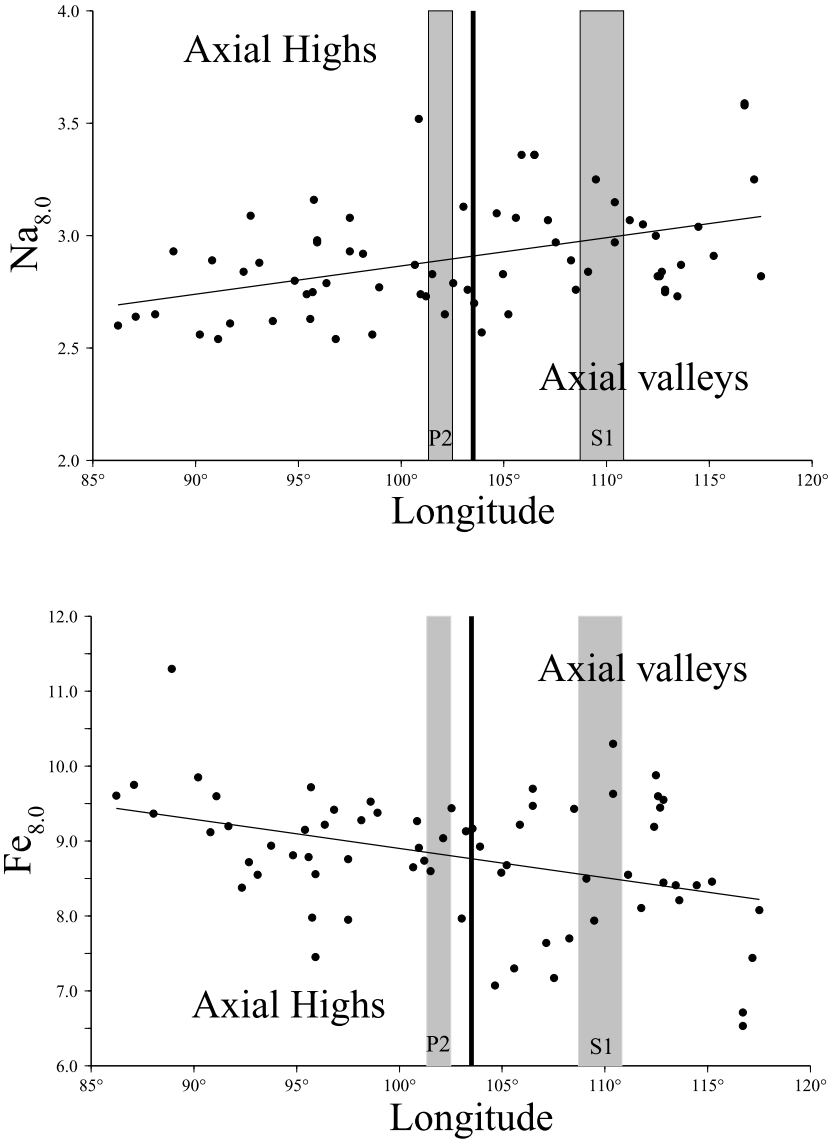

Figure 2. Variation of $Na_{8.0}$ (top panel) and $Fe_{8.0}$ (bottom panel) along the Southeast Indian Ridge as a function of longitude. Thin lines show linear least-squares fits to the data. Heavy vertical line shows the location of the fundamental change in the form of the axial morphology within Segment P3. Shaded boxes show the longitude extent of Segments P2 and S1. Data is tabulated in Mahoney *et al.* (2002).

located within a shallow valley (Shah & Sempere 1998; Cochran & Buck 2001).

Segment R is located immediately to the east of a large-offset, left-stepping transform (Fig. 1) and, like Segments P1 and M1, is a leading segment in the hotspot reference frame (Baran *et al.* 2005).

Shallow axial valleys, such as those found between 103°E and 114°E appear to be characteristic of intermediate spreading rate ridges without a steady-state axial magma lens (e.g. Blacic *et al.* 2004; Baran *et al.* 2005). They produce a distinct form of ridge flank morphology distinguished by abyssal hills that are larger than those found at segments with axial highs, but smaller than those on the flanks of segments with a deep axial valley (Goff *et al.* 1997; Ma & Cochran 1997).

Segment T, extending from 114°22′E to 115°30′E is characterized by a deeper (1000–1200 m) rift valley. This segment has been referred to as 'MAR-like' (e.g. Cochran *et al.* 1997), but its morphology and gravity anomalies differ significantly from typical MAR segments. In particular, Segment T is not characterized by an intrasegment bathymetry high and mantle Bouguer gravity anomaly (MBA) low as typically found at segments on the MAR. Its morphology appears similar to that of Segment B5W in the eastern AAD (Palmer *et al.* 1993).

DATA

An MCS reflection and OBH wide-angle reflection/refraction study of the axial region of the SEIR from 100°E to 116°E was carried out during *R/V Maurice Ewing* cruise EW0114 during the Austral summer of 2001 and 2002. The MCS seismic reflection experiment consisted of an along-axis profile, numerous across-axis lines and an axis-parallel line along the 550 ka isochron (∼20 km from the axis) on the southern flank of Segments P1, P2 and S1 (Figs 3 and 4). Along-axis seismic reflection lines were also obtained in Segments P3, P4 and R. Detailed information on instrumentation, data collection and data reduction is given by Baran *et al.* (2005).

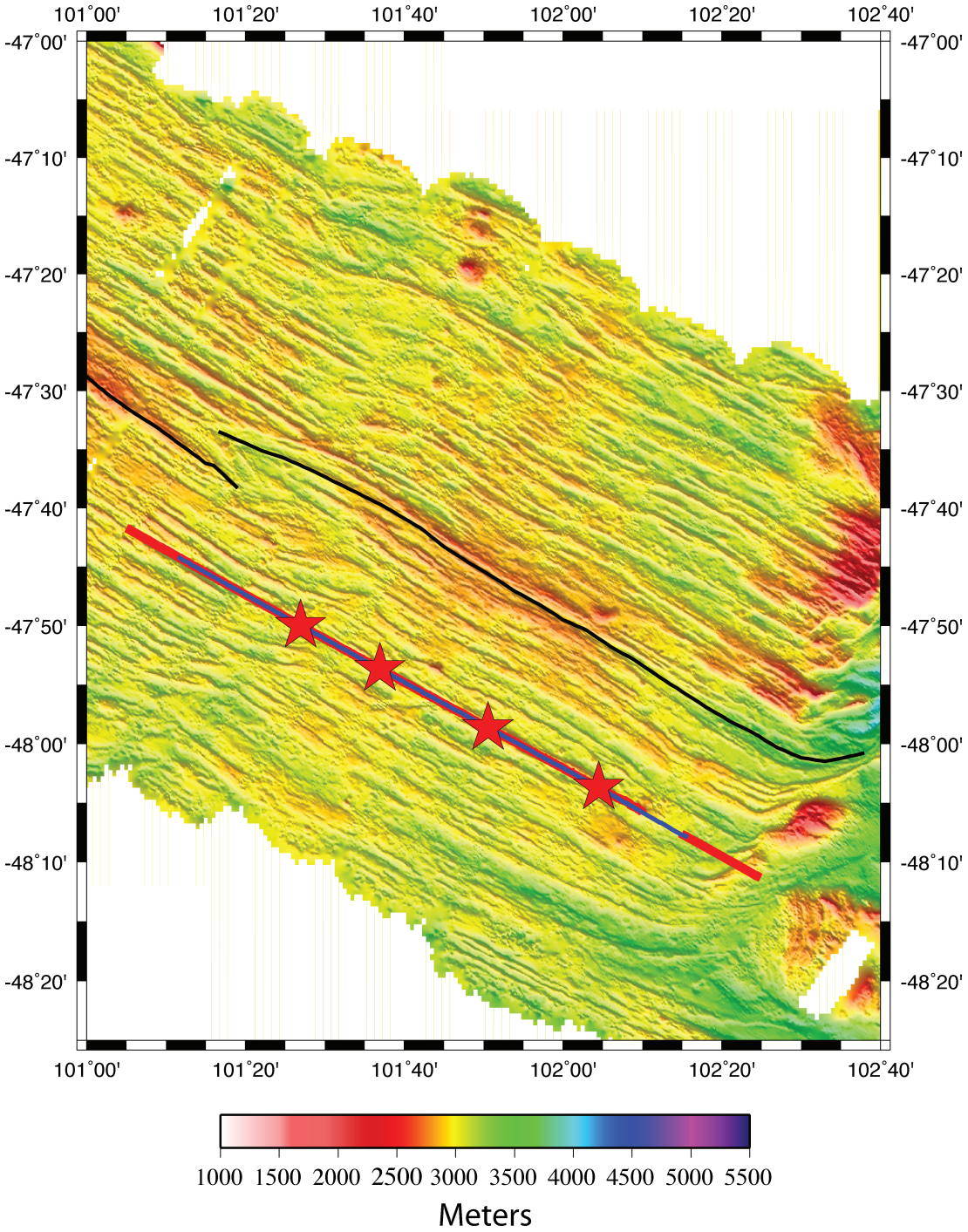

Figure 3. Shaded relief multibeam swath bathymetry map of SEIR Segment P2. Red line and red stars show the ship track and OBH locations for the seismic refraction line (Holmes *et al.* 2008) used to define crustal thickness and seismic velocity structure. Blue line shows the ship track for the MCS line (Baran *et al.* 2005, 2009) used to determine layer 2A thickness and average velocity. Black line shows the location of the ridge axis. Bathymetry is illuminated from the SSW.

The OBH experiment consisted of along-axis wide-angle reflection/refraction profiles in Segments P1, P2, S1 and T. Axis-parallel lines were also run along the 550 ka isochron on the southern flank of Segments P1 and P2. Atrocious weather and sea conditions prevented off-axis refraction experiments in Segments S1 and T as well as the collection of any MCS data in Segment T. Each refraction experiment utilized four OBHs spaced at 15–20 km intervals. The shooting lines were 104–127 km long and extended for at least 20 km beyond the last OBH at each end (Figs 3 and 4). All of the OBH lines (other than the one in Segment T) coincided with MCS reflection lines. MCS reflection and OBH refraction data were collected on separate passes along the same line since the optimal shooting interval for the two experiments is different. Detailed information on the collection and processing of the OBH data as well as a detailed uncertainty analysis is given by Holmes *et al.* (2008). Holmes *et al.* (2008) also presents profiles showing the variation

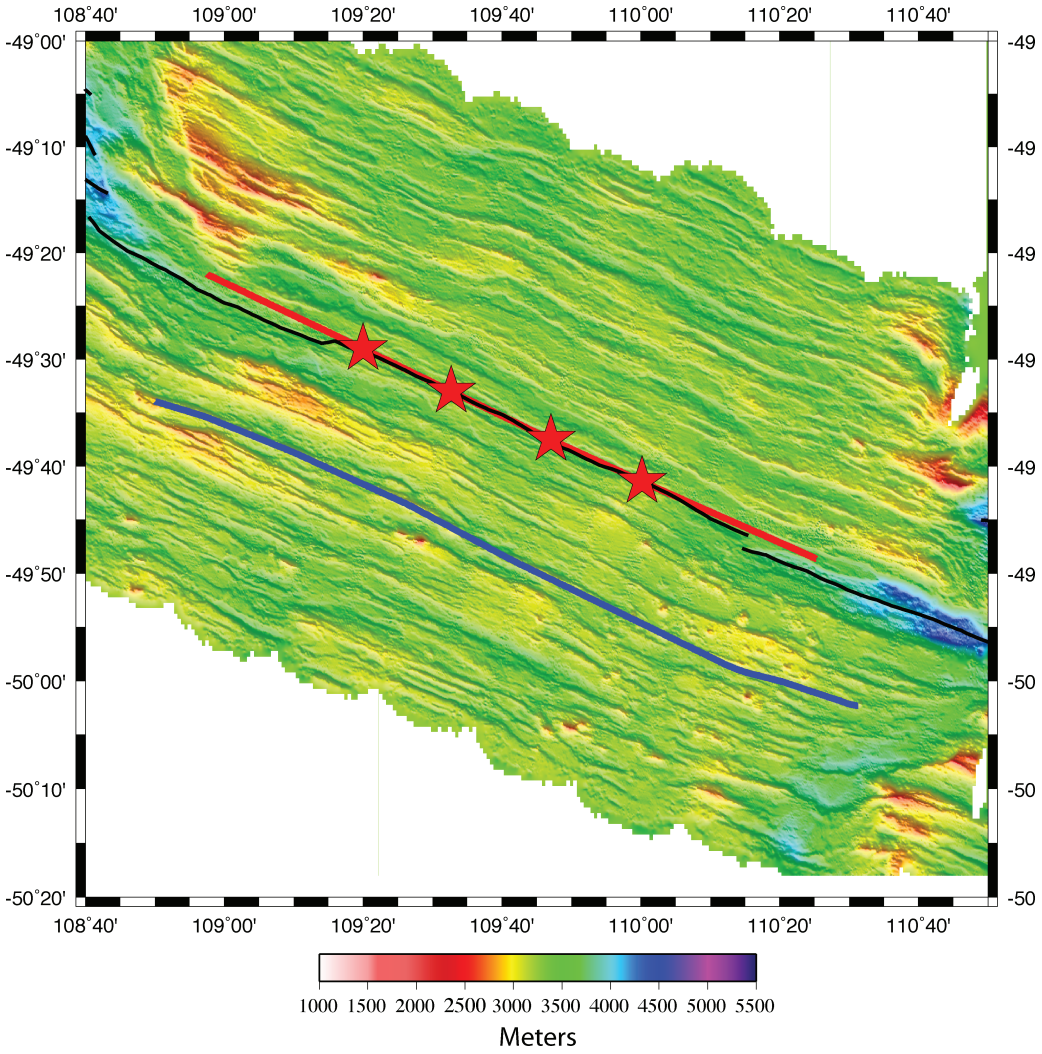

Figure 4. Shaded relief multibeam swath bathymetry map of SEIR Segment S1. Red line and red stars show the ship track and OBH locations for the seismic refraction line (Holmes *et al.* 2008) used to define crustal thickness and seismic velocity structure. Blue line shows the ship track for the MCS line (Baran *et al.* 2005, 2009) used to determine layer 2A thickness and average velocity. Black line shows the location of the ridge axis. Bathymetry is illuminated from the SSW.

in velocity structure and crustal thickness along each of the OBH lines.

In this study, we concentrate on data from the lines located 20 km from the axis on 550 ka crust in order to avoid dynamic and thermal effects of axial processes. These lines are located on the ridge flank away from the dynamically supported axial topography. Also, hydrothermal circulation causes transient crustal thermal effects of lithospheric generation to be confined to the immediate area of the ridge axis (e.g. Dunn *et al.* 2000; Cochran & Buck 2001).

We investigate two segments with differing axial morphology in this study: P2 with a rifted axial high and S1 where the axis is within a shallow axial valley (Figs 3 and 4). Segment P2, extending for 105 km from about 101°20′E to 102°40′E (Fig. 3), is the first complete segment to the west of the transition in axial morphology near 103°30′E within Segment P3. It is characterized by an axial high that is 15–20 km wide, but only 100–200 m high and cut by small, inward-facing faults, so the axis sits in a shallow, ∼50 m deep graben superimposed on the axial high (Cochran *et al.* 1997; Shah & Sempere 1998; Fig. 3). This morphology is typical of the SEIR axis from 79°E to 103°E. An axial magma chamber (AMC) was imaged beneath 20 per cent of Segment P2 at a depth of about 2100 m below the seafloor (Baran *et al.* 2005). However, the seismic reflection data are noisy due to very bad weather and the AMC reflection is difficult to identify. Attenuation of arrivals on the along-axis refraction line suggests that the magma lens is more extensive and may be present under much of the segment. As a result, Holmes *et al.* (2008) were unable to obtain a reliable crustal thickness estimate from the axial refraction line in Segment P2. The mean crustal thickness based on the seismic refraction line along the 550 ka isochron is 5.9 ± 0.2 km (Holmes *et al.* 2008; Fig. 5A).

Segment S1 extends for 165 km from 108°40′E to 110°50′E (Fig. 4), approximately 425–590 km east of the 103°30′E transition in morphology. The axis is located within a shallow 200–600 m deep valley that deepens near the ends of the segment, particularly towards a propagating rift tip at the eastern end of the segment (Fig. 4). No magma lens is imaged in the MCS data and there is no significant attenuation of arrivals travelling along the axis in the OBH data to suggest the presence of a magma lens (Holmes *et al.* 2008). The mean crustal thickness based on the seismic refraction line along the axis is 5.3 ± 0.3 km (Holmes *et al.* 2008; Fig. 5A).

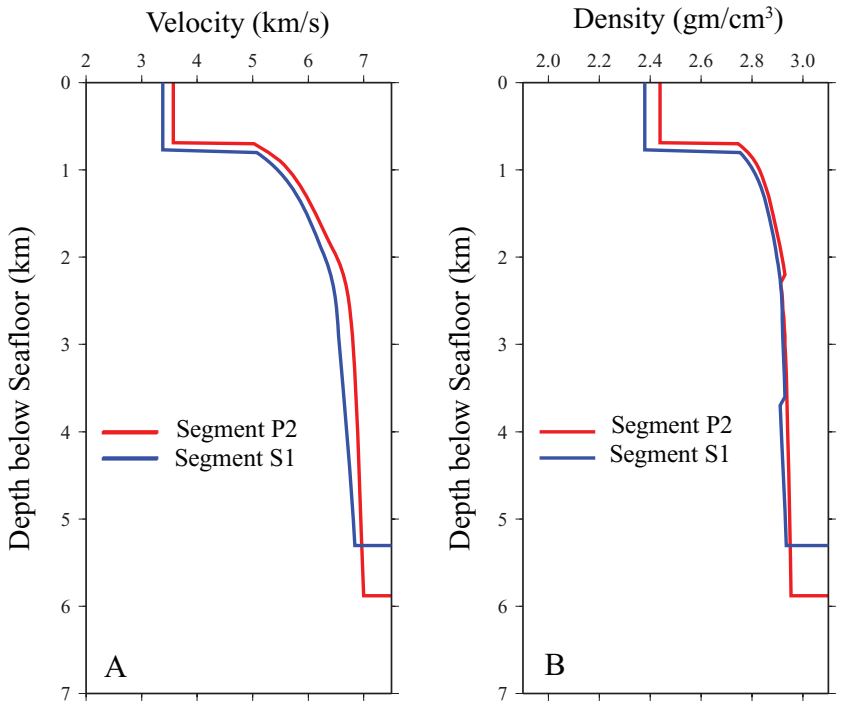

Figure 5. (A) Seismic velocity versus depth profiles for 550 ka crust derived from MCS data (Baran *et al.* 2009) for layer 2a and refraction data (Holmes *et al.* 2008) for the rest of the crust. Red line is for Segment P2 and blue line is for Segment S1. (B) Density-depth profiles derived from the velocity profiles shown in (A) using the Carlson & Raskin (1984) velocity–density relationship.

AXIS-PARALLEL MANTLE TEMPERATURE GRADIENT

The long-wavelength gradient in depth along the SEIR results from the isostatic effects of both the along-axis mantle temperature gradient and changes in crustal thickness. The two are related since melt production and thus crustal thickness depends on the mantle temperature (e.g. McKenzie 1984; Klein & Langmuir 1987). However, it is not possible to simply use the increase in depth along with melt production models to determine the temperature gradient since the variation in water depth also depends on the depth to which density variations in the mantle extend. The availability of crustal thickness and seismic velocity information from segments on either side of the transition in morphology (Holmes *et al.* 2008) allows us to quantify the mantle temperature variation between those segments and to determine the depth to which it extends. We first use the seismic velocities to determine the distribution of density within the crust in Segments P2 and S1. Isostatic compensation of the resulting crustal density structure assuming Airy isostasy and a constant density mantle explains only a portion of the difference in depth between the two segments. We then determine the mantle density difference (and thus temperature difference) required to isostatically balance the two segments as a function of the compensation depth. The actual temperature and density variation between the two segments is estimated from a variety of melt models relating crustal thickness and mantle temperature. Determination of the temperature difference defines the density difference and thus the compensation depth. Finally, we test whether the inferred density structure is compatible with observed gravity data from the SEIR.

Depth variation

The mean water depth for the MCS line along the axis in Segment P2 is 2895 m, while the mean water depth along the axial MCS line in Segment S1 is 3461 m. However, a large portion of the 566 m change in mean axial depth between the two segments results from the difference in the form of the axial morphology, which is dynamically supported (e.g. Tapponnier & Francheteau 1978; Chen & Morgan 1990a,b; Shah & Buck 2001). We wish to compare the mean water depth along the off-axis refraction lines. In order to average out depth variations due to abyssal hill relief, we determined the mean depths over a 10 km-wide swath centred on the MCS lines along the 550 ka isochron and extending the length of the lines (blue lines in Figs 3 and 4. The mean depths are 2996 $\pm$ 68.5 m in Segment P2 and 3194 $\pm$ 120.5 m in Segment S1, so the difference in mean ridge flank depth is 198 m. The difference in standard deviations at the two segments is directly related to differences in the height of the abyssal hills contained in the 10 km-wide swaths (Goff *et al.* 1997; Ma & Cochran 1997).

Crustal density structure

We use the velocity structure determined from the OBH line along the 550 ka isochron to determine the crustal density and thickness in Segment P2 (Fig. 5) for the isostatic calculations. A refraction line along the 550 ka isochron was not obtained in Segment S1 because of weather and sea conditions. We therefore use the crustal velocity structure determined from the OBH line along the axis (Fig. 5A). We thus assume no change away from the axis in the crustal thickness or in the density structure below layer 2A. The presence of a well-developed Moho and lack of an axial magma lens or upper crustal low velocity zone on the axial OBH line (Holmes *et al.* 2008) supports this assumption. In both of the crustal velocity profiles in Fig. 5A, the average layer 2A thickness and velocity determined from MCS data along the 550 ka isochron line (Baran *et al.* 2005, 2009) is combined with refraction results (Holmes *et al.* 2008) for the deeper crust.

We convert velocity to density using relationships determined by Carlson & Raskin (1984) based on rock samples from ODP drilling and ophiolites. For velocities less than 6.65 km s^{-1}, density is given by

$$\rho = 3.50 - 3.79/V_p, \quad (1)$$

where ρ is density in gm cm^{-3} and V_p is the compressional velocity in km s^{-1} (Carlson & Raskin 1984). For crustal rocks with V_p greater than 6.65 km s^{-1}, Carlson & Raskin (1984) give the density by

$$\rho = 3.81 - 5.99/V_p. \quad (2)$$

The two equations are independently constrained, resulting in a small negative jump in the calculated density at $V_p = 6.65$ km s^{-1}. Profiles of density versus depth at Segments P2 and S1 are shown in Fig. 5(B).

Isostatic modelling

If a constant mantle density of 3.33 g cm^{-3} is assumed, the differing crustal thickness and density structure of Segments P2 and S1 would result in a 33 m difference in water depth, assuming Airy isostasy. The observed difference in water depth is 198 m, so variations in mantle density must contribute to the isostatic balance.

Fig. 6(A) shows the calculated mantle density beneath Segment P2 as a function of compensation depth that is necessary to isostatically balance mass columns in the two segments assuming Airy isostasy and using the observed mean ridge flank water depths and the crustal density profiles shown in Fig. 5(B). A mantle density of 3.33 g cm^{-3} was assumed beneath Segment S1 and the density of seawater was assumed to be 1.03 g cm^{-3}. The difference in mantle density between the two segments required for isostatic balance is quite large for shallow compensation depths, but rapidly becomes small as the depth of compensation increases. In Fig. 6(B), the difference in mantle density has been converted to temperature difference assuming that the mantle coefficient of thermal expansion is 3.2×10^{-5} $^{\circ}C^{-1}$ (Parsons & Sclater 1977).

Crustal thickness models and mantle temperature variations

Mantle temperature is a primary variable affecting melt production and thus crustal thickness at mid-ocean ridges. A number of studies have investigated the relationship between mantle temperatures and melt production for various melt models and flow regimes. Fig. 7 shows crustal thickness versus mantle temperature relationships obtained by Shah & Sempere (1998) from three different formulations. These are the isentropic model of McKenzie (1984) utilizing two different solidus relationships, the pressure release model of Klein & Langmuir (1987) and the 2-D numerical passive corner flow model of Chen (1996). The horizontal lines in Fig. 7 mark the seismically determined mean crustal thickness at Segments P2 and S1. The vertical lines mark the temperatures at which those lines intersect the different temperature versus crustal thickness curves. Thus, the separation between each set of vertical lines gives an estimate of the mantle temperature difference between the two segments according to that model. The temperature difference is 7 °C for the McKenzie (1984) model with solidus 1, and is in the range of 11–13.5 °C for the other three models. Because of the agreement of these three estimates arrived at by different methodologies, we will assume that the mantle temperature difference between Segments P2 and S1 is in the range of 11–13.5 °C.

The isostatic modelling shown in Fig. 6 then requires that the difference extend to a depth of about 270–330 km.

Gravity anomalies

We examined whether our results are consistent with gravity data by comparing the difference in MBA at the two locations implied by our inferred density structure with the observed change in MBA gravity. The difference in the average MBA measured along the 550 ka isochron MCS lines in Segments P2 and S1 is 16.1 mGal (Cochran *et al.* 1997). For each segment, we determined the MBA anomaly resulting from the difference between our deduced density structure and that assumed by Cochran *et al.* (1997) in their MBA calculation. In these calculations, the crust in each of the

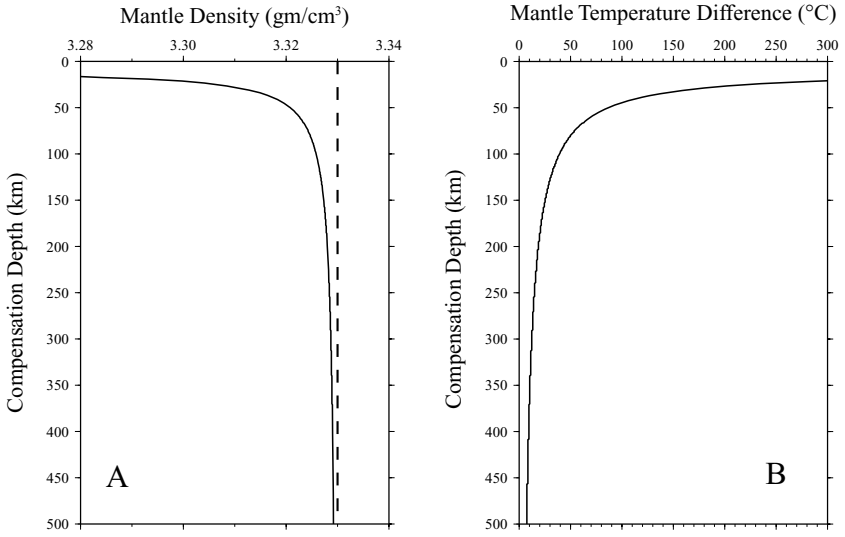

Figure 6. (A) Density of the mantle at Segment P2 necessary to isostatically balance the crustal sections shown in Fig. 5, assuming Airy isostasy, as a function of compensation depth if the mantle density beneath Segment S1 is assumed to be 3.33 g cm^3. (B) Mantle temperature difference between Segments P2 and S1 as a function of compensation depth determined from the density differences shown in (A).

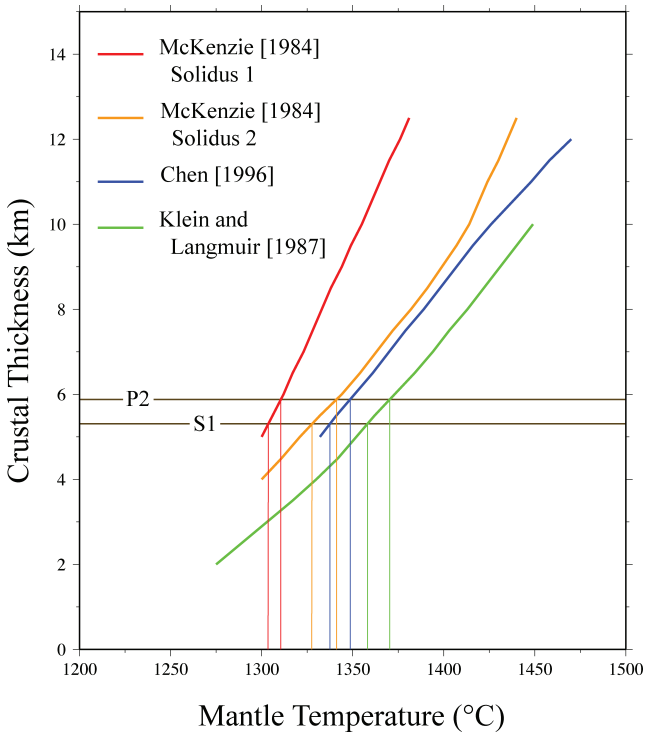

Figure 7. Theoretical relationships between mantle solidus temperatures and crustal thickness from Shah & Sempere (1998). Models shown are from McKenzie (1984), Chen (1996) and Klein & Langmuir (1987). For the McKenzie (1984) models, solidus 1 is given by $T = 1100\ ^\circ\mathrm{C} + P \times 100\ ^\circ\mathrm{C\ GPa^{-1}}$ and solidus 2 is given by $T = 1115\ ^\circ\mathrm{C} + P \times 120\ ^\circ\mathrm{C\ GPa^{-1}}$. Solid horizontal lines show the crustal thickness observed for Segments P2 and S1 and the vertical lines show the inferred mantle temperature beneath the segments for each relationship.

segments was assumed to have the density structure shown for it in Fig. 5(B). A mantle density difference of 1.305×10^{-3} g cm^{-3}, corresponding to a temperature difference of 12.25 °C, was assumed to extend to a depth of 300 km, which is the depth necessary to isostatically balance the two sections with Airy isostasy (Fig. 6). The resulting calculated difference in MBA between the two locations is 15.4 mGal, in reasonable agreement with the observed difference.

VARIABLE ASTHENOSPHERIC THICKNESS MODEL

As discussed above, geophysical and geochemical data along the SEIR are consistent with an along-axis upper mantle temperature gradient approaching the AAD. However, an alternative model has been proposed by Buck *et al.* (2003, 2009) that assumes a constant asthenosphere temperature but varies the asthenospheric thickness along the ridge axis. Their model assumes a distinct asthenospheric layer that floats on a slightly denser mantle mesosphere and is overlain by much denser lithosphere. According to this model, when rifting began between Antarctica and Australia, only mesospheric mantle was available to fill the rift from below. The thick lithospheric roots beneath the two continents also limited inflow of warmer, more easily melted asthenosphere to be from the two ends of the rift. As asthenosphere flows into the region between the two continents, it is consumed by lithosphere creation at the ridge axis with the result that the asthenosphere thins towards the AAD, perhaps approaching zero thickness.

In this model, the depth variation approaching the AAD is partially due to thinning of the less dense asthenospheric layer and partially due to changes in crustal thickness. The change in crustal thickness arises because the zone of melt production is totally within the asthenosphere away from the AAD, but as the AAD is approached, it will be partially within the cooler mesosphere which will produce less melt. If the density difference between the asthenosphere and mesosphere is 0.01 g cm^{-3} (equivalent to a temperature difference of 100 °C) as assumed by Buck *et al.* (2009), then isostatic balance requires that the asthenosphere is 39.5 km thinner under Segment S1 than under Segment P2.

However, the models of Buck *et al.* (2009) require an average asthenospheric thickness of 250–300 km and in their models that reproduce the along-axis depth variation on the SEIR, the axial asthenospheric thickness in the region from 103°E to 110°E considered in our study is more than 150 km. Since normal asthenosphere may begin to melt at 100–150 km (e.g. Klein & Langmuir 1987), a decrease in crustal thickness should be confined to areas of thinner lithosphere nearer to the AAD, with the eastward increase in axial depths in our study area due entirely to shallowing of the asthenosphere-mesosphere boundary. This is inconsistent with the systematic west-to-east thinning of the crust observed along this section of the SEIR (Holmes *et al.* 2008).

DISCUSSION

Holmes *et al.* (2008) found that the average crustal thickness of all four segments in which refraction experiments were carried out fall closely on a linear trend with distance along the axis. Since the melt production curves in Fig. 7 are approximately linear over the range of crustal thicknesses observed on the SEIR (4.6–6.1 km), we will therefore assume a linear temperature gradient between Segments P2 and S1. With this assumption, a temperature change of 12 °C across the 610 km from the centre of P2 to the centre of S1 implies that the mantle temperature change across Segment P3, in which the transition occurs, is 2.4 °C.

In addition, the change in morphology and crustal structure is very abrupt occurring over a narrow zone within a single segment over which the transition is complete. The only area to the east of 103°30′E to the AAD with an axial high morphology is the western portion of Segment R. Segment R is a leading segment in the hotspot frame (Gripp & Gordon 1990) and leading segments show unusual magmatic vigor along the entire SEIR (Baran *et al.* 2005) and at other ridges (Carbotte *et al.* 2004). The only segment to the west of 103°30′E to near the Amsterdam-St Paul's Plateau with an axial valley is Segment N which is a relatively short 55-km-long segment bounded at both ends by transform faults. Horizontal heat flow across transform faults can result in lowered temperatures immediately below the adjacent ridge axis and this reduced melt production (e.g. Prince & Forsyth 1988). In both cases, the segment providing the exception is well away from the transition and in a position where plate boundary geometry allows factors other than mantle temperature to influence melt production.

The change in axial and ridge flank morphology within Segment P3 on the SEIR is also accompanied by abrupt changes in other observable parameters including abyssal hill heights (bathymetric roughness) (Ma & Cochran 1996, 1997; Goff *et al.* 1997), magnetic anomaly amplitude (Ma & Cochran 1996), layer 2a thickness both on-axis (Baran *et al.* 2005) and off-axis (Baran *et al.* 2009), and the presence or absence of an AMC reflection (Baran *et al.* 2005). The sudden transformation in a large number of parameters over a very

small change in mantle temperature strongly suggests a threshold change between two very different, distinct and stable modes of crustal generation. The controlling factor appears to be whether or not it is possible to maintain a steady-state axial magma lens. This is supported by the observation that an axial magma chamber is observed beneath the portion of Segment R with an axial high (Baran *et al.* 2005).

These observations are consistent with numerical models of crustal generation that include the effects of hydrothermal circulation and injection of melt into a crustal magma lens at a depth defined by axial depth of the melt solidus (Phipps Morgan & Chen 1993; Chen & Phipps Morgan 1996; Chen 2000). In these models, the ridge axis thermal structure and crustal accretion process are controlled by the interplay of the heat delivered by new magma and hydrothermal cooling. In particular, Chen (2000) investigated the effects of variations in mantle temperature on crustal accretion and ridge axis thermal structure. He found that at a given spreading rate, there is a narrow range of mantle temperatures over which the axis goes from having an axial magma lens to not be able to support a lens. The rapid transition is largely due to the buffering effect of the latent heat, assumed to be released within the magma lens (Chen & Phipps Morgan 1996; Chen 1996).

The rapid change from an axial magma lens to no lens means that the small decrease in mantle temperatures is accompanied by a large change in the crustal thermal structure both because hot melt is not emplaced within the crust and because hydrothermal circulation can penetrate deeper. With a strongly temperature dependent rheology (Kirby 1983), the very different temperature structures with and without the magma lens will also result in very different forms and distribution of faulting near the axis.

Axial valleys and axial highs thus appear to characterize two distinct modes of crustal generation. Observations from the SEIR also suggest that the rifted axial high characteristic of intermediate spreading ridges grades into the 'EPR-like' axial high found at fast spreading ridges with the controlling parameter being the depth to the magma lens (Baran *et al.* 2005). It is unclear whether the shallow axial valley morphology observed on the SEIR and commonly found at other intermediate spreading rate ridges is distinct from or grades into the deep axial valley observed at the MAR. The presence of an abrupt increase in valley depth between Segments S4 and T on the SEIR accompanied by a step in ridge flank roughness (Goff *et al.* 1997; Ma & Cochran 1997) and a step in the base level of the MBA anomalies (Cochran *et al.* 1997) appear to suggest the presence of two distinct modes. However, as discussed above, Segment T is not a typical 'MAR-like' segment, so this issue remains open.

CONCLUSIONS

Ridge axis and ridge flank depths along the SEIR systematically increase from 90°E to 120°E approaching the AAD. The increase in depth is accompanied by a sudden change in axial morphology near 103°30′E from an axial high in the west to an axial valley in the east. The change in axial morphology is not related to a change in spreading rate, which is nearly constant throughout the area. We have used the results of recent seismic experiments (Baran *et al.* 2005; Holmes *et al.* 2008) along with isostatic considerations to quantify the temperature gradient along the SEIR. The principal results of the this study are:

(1) Seismic refraction experiments show a mean crustal thickness of 5.9 km for Segment P2 characterized by an axial high and a mean crustal thickness of 5.3 km for Segment S1 with an axial valley. Isostatic compensation of the difference in crustal thickness and density structure accounts for only 33 m of the 198 m difference in ridge flank depth between the two segments. The remaining difference in depth appears to result from a gradient in mantle density resulting from a temperature gradient.

(2) Melt generation models imply that a difference in mantle temperature of 11–13.5 °C is required between the two segments to produce the observed difference in crustal thickness. Isostatic compensation of the two segments requires that the resulting difference in mantle density beneath the two segments extend to a depth of about 300 km. The resulting density structure is compatible with the observed gravity anomalies.

(3) The change in axial morphology along the SEIR is very sharp and occurs within a single segment. Assuming a linear mantle temperature gradient between Segments P2 and S1, the change in mantle temperature across that segment (Segment P3) is 2.4 °C. The change in the form of the axial morphology within Segment P3 is accompanied by abrupt changes in a number of observable parameters including abyssal hill height, magnetic anomaly amplitude, on- and off-axis thickness of layer 2A and the presence of absence of a magma chamber. These observations strongly suggest an abrupt threshold change between two distinctly different modes of crustal generation. The trigger for the change between the two modes appears to be whether a steady-state axial magma lens can be maintained.

ACKNOWLEDGMENTS

Discussions with and suggestions from Roger Buck and Mladen Nedimovic contributed greatly to this work. Comments and suggestions from Y. John Chen and an anonymous reviewer were extremely helpful. The efforts of the Captain, crew and scientific staff aboard *R/V Maurice Ewing* under very difficult weather and sea conditions were essential to the collection of the data utilized in this study. The GMT software package (Wessel & Smith 1998) was used for the preparation of figures. This work was supported by National Science Foundation grant OCE-99–11720. LDEO contribution 7278.

REFERENCES

Baran, J.M., Cochran, J.R., Carbotte, S.M. & Nedimovic, M., 2005. Variations in upper crustal structure due to a mantle temperature gradient along the Southeast Indian Ridge, *Geochem. Geophys. Geosyst.,* **6,** Q11002, doi:1029/2005GC000943.

Baran, J.M., Carbotte, S.M., Cochran, J.R. & Nedimovic, M., 2009. Upper crustal seismic structure along the Southeast Indian Ridge from 0 to 550 ka, *Geochem. Geophys. Geosyst.,* in press.

Blacic, T., Ito, G., Canales, J.P., Detrick, R.S. & Sinton, J., 2004. Constructing the crust along the Galapagos Spreading Center at 91.3°–95.5°W: correlation of seismic layer 2A with axial magma lens and topographic characteristics, *J. geophys. Res.,* **109,** B10210, doi:10.1029/2004JB003066.

Buck, W.R., Small, C., Ryan, W.B.F., Carbotte, S.M., Muhlenkamp, B.M. & Haxby, W.F., 2003. Constraints on asthenospheric flow from the depth of oceanic spreading centers, *EOS Trans. Am. Geophys. Un.,* **84**(6), Fall Meet. Suppl. Abstract T52E-06, F1464.

Buck, W.R., Small, C. & Ryan, W.B.F., 2009. Constraints on asthenospheric flow from the depths of spreading centers: the East Pacific Rise and the Australian-Antarctic Discordance, *Geochem. Geophys. Geosyst.,* in press.

Carbotte, S.M., Small, C. & Donnelly, K., 2004. The influence of ridge migration on the magmatic segmentation of mid-ocean ridges, *Nature,* **429,** 743–746.

Carlson, R.L. & Raskin, G.S., 1984. Density of the oceanic crust, *Nature,* **311,** 555–558.

Chen, Y.J., 1996. Constraints on melt production rate beneath the mid-ocean ridges based on passive flow models, *Pure appl. Geophys.,* **146,** 589–620.

Chen, Y.J., 2000. Dependence of crustal accretion and ridge-axis topography on spreading rate, mantle temperature, and hydrothermal cooling, in *Ophiolites and Oceanic Crust: New Insights from Field Studies and the Ocean Drilling Program,* eds Dilek, Y., Moores, E.M., Elthon, D. & Nicolas, A., pp. 161–179, Geol. Soc. Am. Spec. Paper 349, Boulder, CO.

Chen, Y.J. & Morgan, W.J., 1990a. Rift valley/no rift valley transition at mid-ocean ridges, *J. geophys. Res.,* **95,** 17 571–17 581.

Chen, Y.J. & Morgan, W.J., 1990b. A non-linear rheology model for mid-ocean ridge axis topography, *J. geophys. Res.,* **95,** 17 583–17 604.

Chen, Y.J. & Phipps Morgan, J., 1996. The effects of spreading rate, the magma budget, and the geometry of magma emplacement on the axial heat flow at mid-ocean ridges, *J. geophys. Res.,* **101,** 11 475–11 482.

Cochran, J.R. & Buck, W.R., 2001. Near-axis subsidence rates, hydrothermal circulation and the thermal structure of mid-ocean ridge crests, *J. geophys. Res.,* **106,** 19 233–19 258.

Cochran, J.R., Sempere, J.C. & SEIR-Scientific-Team, 1997. The Southeast Indian Ridge between 88°E and 120°E: gravity anomalies and crustal accretion at intermediate spreading rates, *J. geophys. Res.,* **102,** 15 463–15 487.

DeMets, C., Gordon, R.G., Argus, D.F. & Stein, S., 1994. Effect of recent revisions to the geomagnetic reversal time scale on estimates of current plate motions, *Geophys. Res. Lett.,* **21,** 2191–2194.

Dunn, R.A., Toomey, D.R. & Solomon, S.C., 2000. Three-dimensional seismic structure and physical properties of the crust and shallow mantle beneath the East Pacific Rise at 9°30'N, *J. geophys. Res.,* **105,** 23 537–23 555.

Forsyth, D.W., Ehrenbard, R.L. & Chapin, S., 1987. Anomalous upper mantle beneath the Australian-Antarctic Discordance, *Earth planet. Sci. Lett.,* **84,** 471–478.

Goff, J.A., Ma, Y., Shah, A., Cochran, J.R. & Sempere, J.-C., 1997. Stochastic analysis of seafloor morphology on the flanks of the Southeast Indian Ridge: the influence of ridge morphology on the formation of abyssal hills, *J. geophys. Res.,* **102,** 15 521–15 534.

Gripp, A.E. & Gordon, R.G., 1990. Current plate velocities relative to the hotspots incorporating the NUVEL-1 global plate motion model, *Geophys. Res. Lett.,* **17,** 1109–1112.

Holmes, R.C., Tolstoy, M., Cochran, J.R. & Floyd, J.S., 2008. Crustal thickness variations along the Southeast Indian Ridge (100°-116°E) from 2-D body wave tomography, *Geochem. Geophys. Geosyst.,* **9**(12), Q12020, doi:10.1029/2008GC002152.

Kirby, S.H., 1983. Rheology of the lithosphere, *Rev. Geophys. Space Phys.,* **21,** 1458–1487.

Klein, E.M. & Langmuir, C.H., 1987. Global correlations of ocean ridge basalt chemistry with axial depth and crustal thickness, *J. geophys. Res.,* **92,** 8089–8115.

Klein, E.M., Langmuir, C.H. & Staudigel, H., 1991. Geochemistry of basalts from the Southeast Indian Ridge, 115°E-138°E, *J. geophys. Res.,* **96,** 2089–2108.

Kojima, Y., Shinohara, M., Mochizuki, K., Yamada, T., Nakahigashi, K. & Kanazawa, T., 2003. Seismic velocity structure in the Australian-Antarctic discordance segment B4 revealed by airgun-OBS experiment, *EOS (Trans. Am. Geophys. Un.),* **84**(46), Fall. Meet. Suppl., Abstract S21F-0396, F1029.

Kuo, B.Y., 1993. Thermal anomalies beneath the Australian-Antarctic Discordance, *Earth planet. Sci. Lett.,* **119,** 349–364.

Ma, Y. & Cochran, J.R., 1996. Transitions in axial morphology along the Southeast Indian Ridge, *J. geophys. Res.,* **101,** 15 849–15 866.

Ma, Y. & Cochran, J.R., 1997. Bathymetric roughness of the Southeast Indian Ridge: implications for crustal accretion at intermediate spreading rate mid-ocean ridges, *J. geophys. Res.,* **102,** 17 697–17 711.

Mahoney, J.J., Graham, D.W., Christie, D.M., Johnson, K.T.M., Hall, L.S. & Vonderhaar, D.L., 2002. Between a Hotspot and a Cold spot: isotopic variation in the Southeast Indian Ridge Asthenosphere, 86°E-118°E, *J. Petrol.,* **43,** 1155–1176.

McKenzie, D., 1984. The generation and compaction of partially molten rock, *J. Petrol.,* **25,** 713–765.

Palmer, J., Sempere, J.C., Christie, D.M. & Phipps Morgan, J., 1993. Morphology and tectonics of the Australian-Antarctic Discordance between 123°E and 128°E, *Mar. geophys. Res.,* **15,** 121–152.

Parsons, B. & Sclater, J.G., 1977. Ocean floor bathymetry and heat flow, *J. geophys. Res.,* **82,** 803–827.

Phipps Morgan, J. & Chen, Y.J., 1993. Dependence of ridge-axis morphology on magma supply and spreading rate, *Nature,* **364,** 706–708.

Prince, R.A. & Forsyth, D.W., 1988, Horizontal extent of anomalously thin crust near the Vema Fracture Zone from the three-dimensional analysis of gravity anomalies, *J. geophys. Res.,* **93,** 8051–8063.

Pyle, D.G., 1994. Geochemistry of mid-ocean ridge basalt within and surrounding the Australian-Antarctic Discordance, *Ph.D. thesis*. Oregon State University, 178 pp.

Scheirer, D.S., Forsyth, D.W., Conder, J.A., Eberle, M.A., Hung, S.H., Johnson, K.T.M. & Graham, D.W., 2000. Anomalous seafloor spreading of the Southeast Indian Ridge near the Amsterdam-St. Paul Plateau, *J. geophys. Res.,* **105,** 8243–8262.

Sempere, J.C., Cochran, J.R. & SEIR-Scientific-Team, 1997. The Southeast Indian Ridge between 88°E and 120°E: variations in crustal accretion at constant spreading rate, *J. geophys. Res,* **102,** 15 489–15 505.

Sempere, J.C., Palmer, J., Christie, D.M., Phipps Morgan J. & Shor, A.N., 1991. Australian-Antarctic discordance, *Geology,* **19,** 429–432.

Shah, A. & Sempere, J.-C., 1998. Morphology of the transition from an axial high to a rift valley at the Southeast Indian Ridge and the relation to variations in mantle temperature, *J. geophys. Res.,* **103,** 5203–5223.

Shah, A.K. & Buck, W.R., 2001. Causes for axial high topography at mid-ocean ridges and the role of crustal thermal structure, *J. geophys. Res.,* **106,** 30 865–30 880.

Tapponnier, P. & Francheteau, J., 1978. Necking of the lithosphere and the mechanics of slowly accreting plate boundaries, *J. geophys. Res.,* **83,** 3955–3970.

Tolstoy, M., Harding, A.J., Orcutt, J.A. & Phipps Morgan, J., 1995. Crustal thickness at the Australian Antarctic Discordance and neighboring Southeast Indian Ridge, *EOS (Trans. Am. Geophys. Un.),* **76,** F570.

Weissel, J.K. & Hayes, D.E., 1974. The Australian Antarctic Discordance: new results and implications, *J. geophys. Res.,* **79,** 2579–2587.

Wessel, P. & Smith, W.H.F., 1998. New improved version of Generic Mapping Tools released, *EOS Trans. Am. Geophys. Un.,* **79,** 579.